Supplementary Information for

Dynamics of a Lipid Vesicle across a Microfluidic Constriction: How do its Membrane Properties and Microenvironment matter?

Tanoy Kahali[1], Devi Prasad Panigrahi[2] and Suman Chakraborty[1,*]

[1]Department of Mechanical Engineering, Indian Institute of Technology, Kharagpur, Kharagpur, West Bengal-721302, India.

[2]Department of Mathematics, University College London, London, WC1H 0AY, UK

* Corresponding author. E-mail: suman@mech.iitkgp.ac.in

1. Details of 3-D Numerical method

The fluid flow is simulated using Lattice Boltzmann method (LBM), where the evolution of the macroscopic fluid flow velocity is modelled using the discrete velocity distribution function $f_i(\mathbf{x},t)$ which evolves according to a set of collision and streaming rules that depend on the collision model and lattice structure. Here, we employ a D3Q19 lattice structure where each lattice point is connected with 18 other lattice points. The Bhatnagar-Gross-Krook approach (Bhatnagar *et al.* 1954) is used for the collision operation, which updates the value $f_i(\mathbf{x},t)$ towards an equilibrium value $f_{i,eq}(\mathbf{x},t)$ according to the following equation

$$f_i^*(\mathbf{x},t) = f_i(\mathbf{x},t) - \frac{f_i(\mathbf{x},t) - f_{i,eq}(\mathbf{x},t)}{\tau}, \quad (1)$$

where $f_i^*(\mathbf{x},t)$ denotes the post-collision value of the velocity distribution function at a given lattice point, τ is the relaxation time parameter which is a function of the kinematic viscosity of the fluid and sonic speed in the medium. The streaming operation can be mathematically represented as,

$$f_i(\mathbf{x}+\mathbf{c_i}\Delta t, t+\Delta t) = f_i^*(\mathbf{x},t), \quad (2)$$

where $\mathbf{c_i}$ denotes the velocity vectors connecting two lattice points. The value of $f_{i,eq}(\mathbf{x},t)$ at a lattice point is computed based on the value of the macroscopic fluid velocity and density at that point. A detailed discussion on the overall simulation approach can be found in the text of Kruger et al. (Krüger *et al.* 2017).

The external forces on the vesicle due to the fluid flow are lumped on the interfacial marker points. Values of the forces on these points are evaluated by interpolating the stress tensor of the fluid at the neighboring lattice points. The vesicle membrane is represented as an immersed interface; whose mesh is independent of the lattice structure of the fluid. The presence of the vesicle is communicated to the surrounding fluid using a force field, which ensures that the no-slip and no-penetration conditions are satisfied on the interface of the vesicle. This method belongs to a broad class of methods known as the Immersed Boundary Method` which was developed originally by Peskin (Peskin 2002). Here, we apply this method using the Multi-Direct Forcing approach (Ota *et al.* 2012). The no-slip and no-penetration boundary conditions on the walls of the microchannel are enforced using the bounce-back method, where the collision step is replaced by a reflection step such that the fluid-particle populations hitting the bounce-back nodes are reflected along the opposite direction. This leads to an impermeable no-slip wall located exactly halfway between the bounce back node and the adjacent lattice point in the fluid.

At the inlet of the microchannel, we enforce the fully developed velocity profile for Stokes flow, and at the outlet, a mass continuity is enforced.

In all the simulations, we set the dimensionless lattice spacing dx to be 0.5, the normalized kinematic viscosity of the carrier fluid v to be equal to 1, and the relaxation parameter τ to be equal to 2. The size of the time step is obtained from the following diffusive scaling law:

$$dt = c_s^{\,2}(\tau - \frac{1}{2})\frac{dx}{v}, \tag{3}$$

where c_s denotes the sonic speed. The stability of the LBM is ensured as $\tau > 0.5$ (Krüger *et al.* 2017) and the results are found to be independent of the values of τ lying between 1 and 2. The material parameters for the vescicle are so chosen such that they fit the best with our experimental data for stretching along the axial coordinate (λ vs. x). The mapping between the simulation parameters and their corresponding physical values is mentioned in table below. All the 3D LBM simulations are performed using the open-source PALABOS package (Latt *et al.* 2020).

Table S1: Mapping between simulation parameters and their physical values for 3D numerical simulation (Kotsalos *et al.* 2019)

Parameters	**Numerical value**	**Physical value**
Grid Spacing (dx)	0.5	0.5 μm
Kinematic Viscosity (v)	1	1 $\mu m^2/\mu s$
Time step (dt)	0.125	0.125 μs
The density of carrier fluid (ρ)	1025	1025 $fg/\mu m^3$
Bending Rigidity of RBC membrane (κ)	1	1 pN μm
Membrane Elasticity according to Skalak's Law (B, C, D)	B = 5, C = 5000, D = 35	B = 5 pN/μm, C = 5000 pN/μm, D = 35 pN/μm
Rayleigh Damping parameters for modelling viscosity (α_D, β_D)	$\alpha_D = 0$, $\beta_D = 0.01$	$\alpha_D = 0$, $\beta_D = 0.01$

PBD Damping ($\kappa_{damping}$)	$\kappa_{damping}$ = 0.6	$\kappa_{damping}$ = 0.6
Volume Conservation constraint (k_{volume})	k_{volume} = 250	k_{volume} = 250

2. (a) SRT dyamics observed from experiments and 3D simulations

This section describes the three different dynamics (stretching, rolling and tumbling) experienced by a singled-out vesicle as it passes through a constricted microfluidic pathway**.** Figure S1 (a-c) illustrates the experimentally observed stretching, rolling, and tumbling dynamics, respectively, as characterized by the evolution of their orientation angles as a function of axial displacement. In figure S1(d), we plot the corresponding results from 3D numerical simulations ofr three different dynamics. The insets in Figure S1 (a-c) depict the shape deformation of vesicles hallmarked by a parameter called deformation index (*DI=a-b/a+b*); where *a,b* are the half major and minor axis lengths of a nearly elliptic vesicle under consideration.

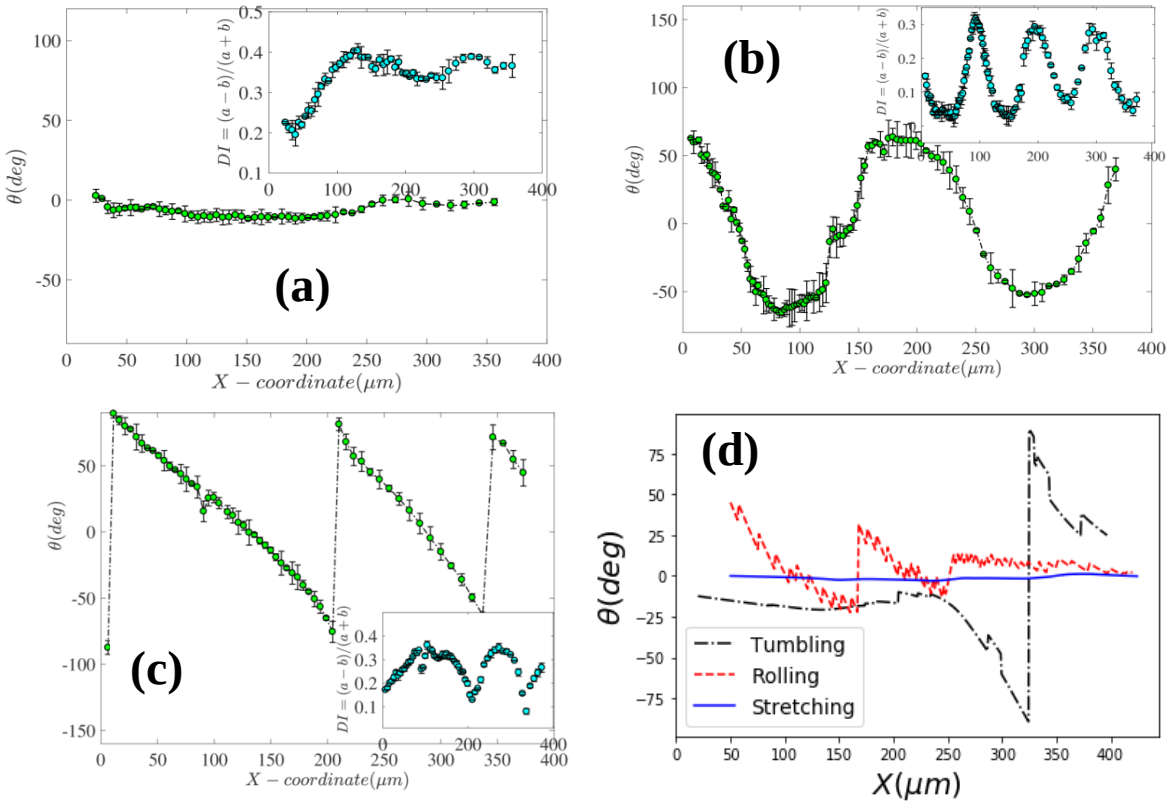

Figure S1. Evolution of orientation angle of a vesicle passing through the constricted section, obtained from experiments (a-c) where (a) is an example of stretching, (b) rolling, and (c) exhibits tumbling, and from 3D numerical simulations (d). Insets of Fig. S1 (a to c) depicts the shape deformation (deviation from initial shape) manifested by the Deformation Index (*DI*) as a function of downstream position(*X*) in the channel.

It can be clearly seen that in the case of tumbling, both experiments (S1(c)) and 3D simulations (black coloured curve in S1(d)) predict a sharp discontinuity in the orientation angle, and this discontinuity goes all the way from -90^0 to 90^0. On the other hand, the stretching regime is characterized by a nearly constant orientation angle which can be seen in both experiments (S1(a)) and simulations (blue coloured curve in S1(d)). In addition to that both the experiments and 3D simulations also predict an intermediate regime, which we call the rolling regime which inherits the characteristics of both tumbling and stretching as can be seen from figure S1(b) and the red curve in figure S1(d). In figure 3 of the main manuscript, we show the results from 2D numerical simulations, along with a comparison with experiments, which in addition to figure S1 establishes the qualitative verification of experiments, 3D LBM simulations and 2D BEM simulations. Since 3D simulations are computationally expensive and we have established that 2D simulations are able to capture the dynamical transitions effectively, we have used 2D simulations for the detailed analysis.

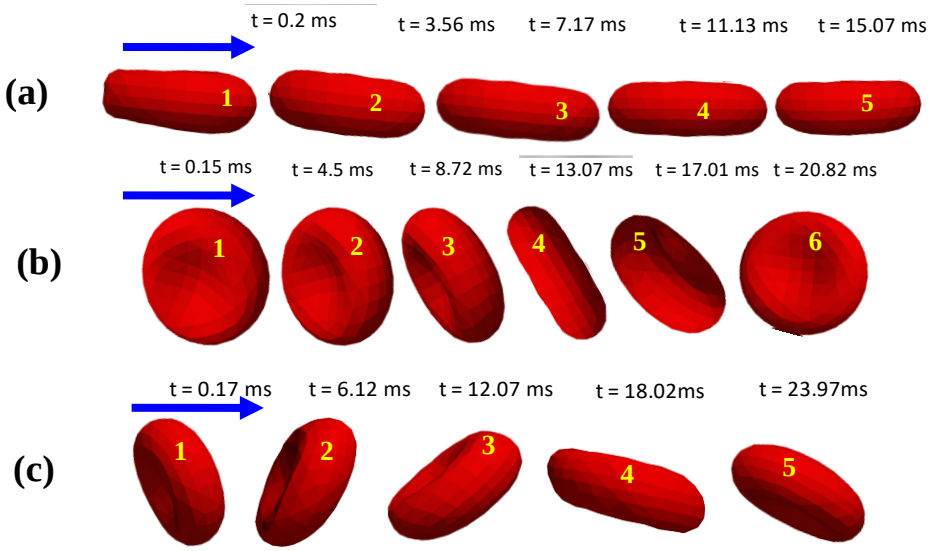

Figure S2. Time-lapse images of an individual vesicle undergoing stretching (a), rolling (b), and tumbling(c) motion while entering a microfluidic constriction, obtained from 3D numerical simulations. The direction of flow is demarcated by balck arrow.

2. (b) Validation of numerical models (both 2-D and 3-D) with experiment:

In the present study we have performed 3D simulations for qualitatively verifying the existence of three dynamical regimes, namely stretching(S), rolling(R) and tumbling(T) in light of the evolution of orientation angle as the vesicle passes through the confinement. Figure S(a-b) represents the evolution of the vesicle orientation angle as a function of axial position and are considered as representative cases for the purpose of validation of both 2D (Fig S.a) and 3D (Fig S.b) simulation results with controlled experiments, depicting good agreement. Further, 3D simulations are computationally expensive which motivates us to decipher and establish the

potential of 2D modelling for effectively probing the dynamical transitions. Hence, we have chosen 2D simulations for the detailed analysis throughout the present study.

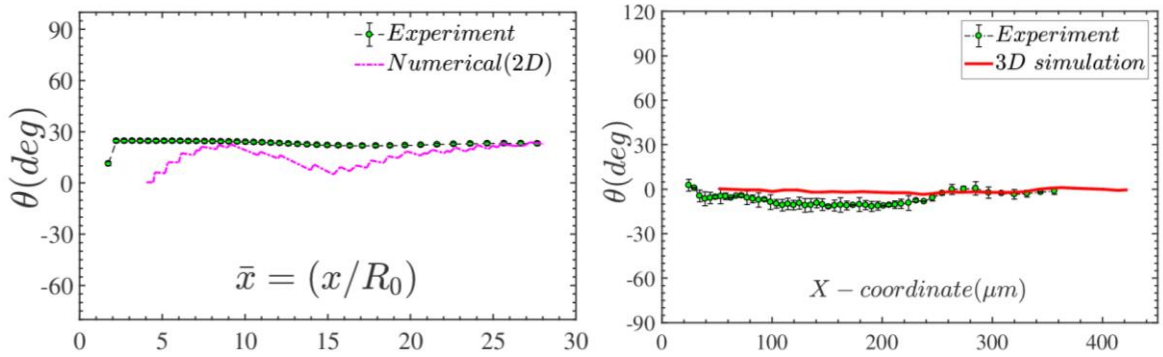

(a) **(b)**

Figure S. Evolution of vesicle orientation angle with axial position for stretching dynamics observed prior to the constriction for: **(a)** 2D model validation ($\tau_{2D} = 0.93$) with experiments ($\nu_{\exp} = 0.97$). (b) 3D model validation ($\tau_{3D} = 0.74; \nu_{\exp} = 0.88$). Open symbols denote the experimental results while lines represent the simulations.

3. Membrane bending modulus estimation from inverse mapping

The inverse mapping method has been used to estimate the value of membrane bending modulus by coupling the numerical and experimental data for a fixed identity vesicle undergoing stretching dynamics while migrating through the tapered region prior to the constriction. The simulations are carried out initially with a guess value of E_B, and the findings from the same in terms of stretch ratio vs. x-position (refer to Figure S3., *inset*) was superimposed with the experimental observation for the similar parametric space for different Glutaraldehyde concentration. An error minimization technique was employed to obtain the desired E_B value resulting in a collapse of experiment and simulation results. The findings are represented in a tabular form (Table S2).

Table S2. Membrane bending modulus as a function of Glutaraldehyde concentration

Gluta. Concentration (% v/v)	Max. stretch ratio	Normalized bending modulus
0	1.315	0.002
5	1.236	0.053
10	1.2	0.084

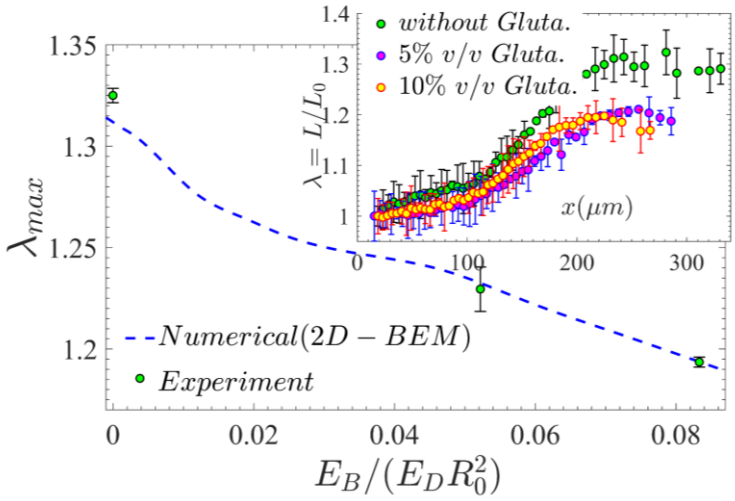

Figure S3. Variation of the maximum value of stretching ratio as a function of normalized membrane bending rigidity modulus for a vesicle undergoing stretching. Inset depicts the evolution of stretch ratio as a function of axial position for different Glutaraldehyde concentrations. It is evident from the inset figure that, with an increase in glutaraldehyde concentrations, the stretching is gradually arrested due to the increment of the bending modulus of the vesicle membrane. The open symbols in the figure demarcate the experimental findings, while the solid lines represent the numerical simulation results.

4. Size distribution of vesicle samples obtained from electroformation

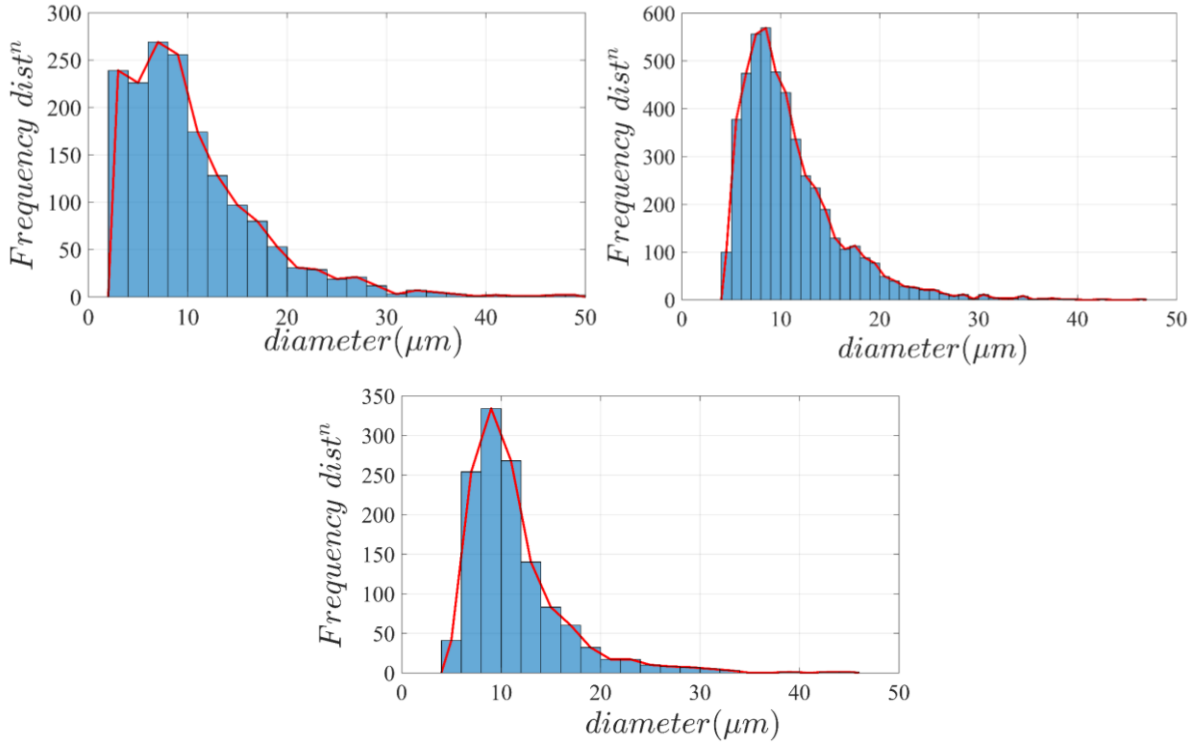

Figure S4. Size distribution of GUV samples obtained from electroformation: The histogram

representsthe variation in vesicle effective diameter ($2R_0$) as a function of its frequency/number obtained from sampling upon (a) 1650 nos. (b) 4605 nos. and, (c) 1261 nos. samples on different days.

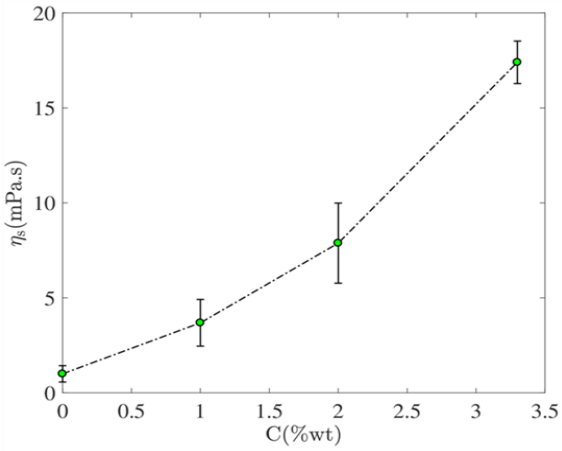

Figure S5. Variation in shear viscosity of the vesicle inner solution (containing Dextran of 500 kDa molecular wt.) as a function of Dextran concentrations at 25^0 C obtained from the rheometry result for the experimentation related to the viscosity contrast study.

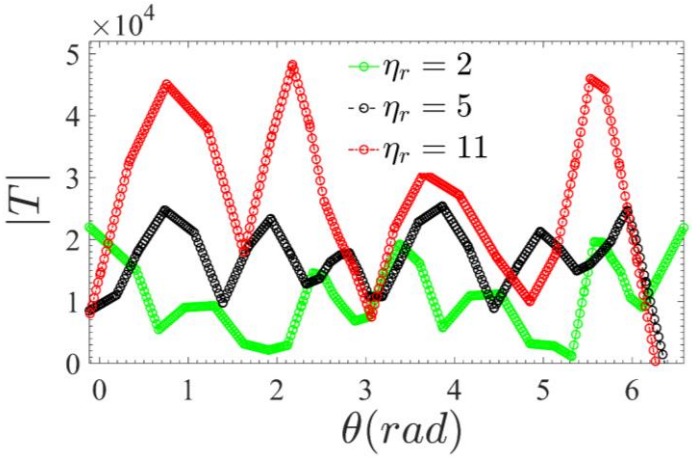

Figure S6. Variation in the magnitude of traction force ($|\boldsymbol{T}|$) on the vesicular interface as a function of the polar angle (θ) for 3 different viscosity ratios, as obtained from numerical simulations. The reduced areas corresponding to η_r =2,5 and 11 are $\tau_{2d} \sim 0.94$.

Table S3. Properties of the working fluids used in lipid-vesicle synthesis

components		Chemicals used	Viscosity (mPas)	Density (Kg/m^3)
Inner-fluid	Case-1	400 mM sucrose-Aq. solution	1.06	984
	Case-2	400 mM sucrose-Aq. solution+1%w/w Dextran	3.685	980

	Case-3	400 mM sucrose-Aq. solution+2% w/w Dextran	7.88	987
	Case-4	400 mM sucrose-Aq. solution+3.3% w/w Dextran	17.4	989
Outer-fluid		435 mM glucose-Aq. solution	0.989	980

5. Explanation for Stretching-Rolling-Tumbling transition:

The parameter $\phi(t)$, denotes the phase angle of an infinitesimal membrane element. In other words, it is the polar angle describing instantaneous angular position of a material surface point located on the membrane surface. The observed shape transitions (Stretching → Rolling →Tumbling) could be rationalized by introducing a parameter $\phi(t)$, denoting the phase angle of an infinitesimal membrane element, so that its time rate of change, $d\phi/dt$ i.e. the angular velocity of the material point on the membrane, which could be linearly mapped with the tank-treading frequency of the observed motion (Keller and Skalak 1982) of a nearly ellipsoidal capsule under consideration. Accordingly, the following inequalities could hold:

$$\left(\frac{d\phi}{dt}\right)_{Tumbling} < \left(\frac{d\phi}{dt}\right)_{Rolling} < \left(\frac{d\phi}{dt}\right)_{Stretching} \tag{1}$$

Now, from pure geometric considerations valid for an encapsulation that may be idealized with an ellipsoidal boundary (Keller and Skalak 1982) and further mapping the same to a 2D representation, eventually simplified the expression to the following:

$$\frac{d\phi}{dt} \sim \frac{1}{r^{-1} - r}, \tag{2}$$

Where, r is the ratio of the minor axis ($2b$) to the major axis (s$2a$) of a nearly ellipsoidal capsule/ vesicle under consideration i.e. $r = b/a$.

From the above-mentioned equation-2, physically a decrease in r would implicate a reduction in $d\phi/dt$, resulting in decrease in equivalent tank-treading frequency of the material point under consideration. Furthermore, a sharp increase in the tank-treading frequency could further be observed as the value of r approached unity (quasispherical capsule), leaving apart the singularity at r =1.

Now, the reduced area in 2D, of a capsule can be defined as

$$\tau_{2d} = \frac{4\pi A_{capsule}}{P^2_{capsule}} \tag{3}$$

Where, $A_{capsule}$ $(=\pi ab)$ and $P_{capsule}$ $(\sim 2\pi\sqrt{(a^2+b^2)/2})$ are the actual area and the perimeter of the capsule under consideration. Plugging in the values in the Eq-3 leads to

$$\tau_{2d} \sim \frac{2}{\left(r + r^{-1}\right)} \tag{4}$$

Hence, it's evident from Eq-2 and Eq-4 that as r reduces, τ_{2d} decreases leading to further decrement of the tank trading frequency i.e. $d\phi/dt$ and vice-versa. The SRT regime map clearly suggests that for a fixed magnitude of the normalized bending modulus of membrane, since τ_{2d} decreases with a decrease in r from pure geometric considerations, it follows that $d\phi/dt$ also decreases with a decrease in τ_{2d}, hallmarking the kinematic evolution during the shape transition events.

Supporting video (.avi) captions

Movie S1: Experimental video on stretching dynamics of a lipid vesicle in Poiseuille flow while passing through the tapered region prior to the constriction.

Movie S2: Stretching dynamics observed via 2-D simulation.

Movie S3: Experimentally observed rolling motion of a vesicle while passing through the tapered region of the microchannel.

Movie S4: Rolling motion observed from 2-D simulation. (not to actual scale)

Movie S5: Experimentally observed the tumbling motion of an equiviscous (η_r ~1) vesicle.

Movie S6: Tumbling motion, illustrated from 2-D simulation. (not to actual scale)

Movies S7, S8, S9: Stretching, rolling and tumbling dynamics exhibited by a vesicle at constriction, obtained from 3D simulations, respectively. (not to actual scale)

Stretching Exp. vs 2D-sim_to scale: This .ppt file depicts comparison beween experiment and 2D simulation (Movie S1 vs. Movie S2) results on stretching dyamics fit to the scale.